Functionality of potato virus Y coat protein in cell-to-cell movement is defined by flexibility of its N terminal region

Anže Vozelj[1,2*], Tjaša Mahkovec Povalej[1], Katja Stare[1], Magda Tušek Žnidarič[1], Katarina Bačnik[1], Valentina Levak[1,2], Ion Gutiérrez-Aguirre[1], Marjetka Podobnik[3], Kristina Gruden[1], Anna Coll[1]†, Tjaša Lukan[1]†[*]

[1]Department of Biotechnology and Systems Biology, National Institute of Biology, Večna pot 121, 1000 Ljubljana, Slovenia

[2]Jožef Stefan International Postgraduate School, Jamova cesta 39, 1000 Ljubljana, Slovenia

[3]Department of Molecular Biology and Nanobiotechnology, National Institute of Chemistry, Hajdrihova 19, 1001 Ljubljana, Slovenia

* Corresponding authors.

Email: anze.vozelj@nib.si, tjasa.lukan@nib.si

† shared last authorship

Abstract

Potato virus Y (PVY) is one of the top ten economically most important plant viruses and responsible for major yield losses. We previously suggested the involvement of the N terminal region of potato virus Y coat protein (CP) in PVY spread. By constructing different PVY N terminal deletion mutants, we here show that deletions of 40 or more amino acid residues from the N terminal region of the CP resulted in the PVY multiplication limited to primary infected cells. Deletion of 26 residues profoundly impaired PVY cell-to-cell movement and prevented systemic PVY spread, while deletions of 19-23 residues allowed delayed systemic PVY spread. Introduced point mutations in the identified region hinder the filaments formation (S21G) and prevent (S21G) or delay (G20P) PVY movement. In addition, the mutants with deletion of more than 23 residues were not able to form full length viral particles in bombarded leaves, which confirms the overall significance of this region also in capsid assembly.

Author summary

Potato virus Y is one of the most economically important plant viruses worldwide, since it causes major yield losses in *Solanaceae*, especially in potato, where it is the causal agent of potato tuber necrosis ringspot disease, negatively impacting tubers quality and significantly reduces potato yield. By constructing different PVY N terminal deletion mutants, we identified the regions of the coat protein that are important for efficient PVY cell-to-cell movement and putative mechanisms supporting it. Furthermore, our findings indicate that potato virus Y N terminal region plays an important role in efficiency of assembly into full length viral particles. Understanding these regions, responsible for cell-to-cell as well as long distance movement, is crucial for economically important plant viruses such as PVY, since dissolving such complex processes will enhance our understanding of the PVY infective cycle and contribute to the development of effective tackling strategies against PVY infections in potato and prevent yield losses.

Introduction

Plants undergo constant exposure to various pathogens and pests, with viruses being the most severe amongst them. Potato virus Y (PVY) is classified amongst the top ten economically most important plant viruses infecting solanaceous crops including potato, tomato, tobacco and pepper (1). PVY is the causal agent of potato tuber necrosis ringspot disease (2), a devastating disease that negatively impacts potato tuber quality and yield (3).

PVY belongs to *Potyvirus* genus. Its genome consists of 9,7-kb positive sense single stranded RNA (+ ssRNA) encoding for single open reading frame (ORF) that is translated into 350 kDa long polyprotein which is cleaved into 10 mature proteins (3). Furthermore, PVY genome contains an additional ORF *pipo*, embedded within the P3 cistron of the polyprotein, that via transcriptional slippage results in production of the so called “Pretty interesting potyviridae ORF” (P3N-PIPO) protein (4).

The majority of potyviral proteins are multifunctional and they altogether contribute to the establishment of successful viral infection, that encompasses multiple steps including transmission by aphids, penetration of viral particles into the cell, virion disassembly, translation, replication, suppression of host defense mechanisms, virion assembly and virus movement from the primary infected cells to neighboring cells and systemic spread (5).

Viral movement is facilitated through plasmodesmata, plant specific structures connecting two adjacent cells that serve as gateways for cell-to-cell movement and contribute to the establishment of systemic infection (6, 7, 8, 9). At least four potyviral proteins, coat protein (CP), cylindrical inclusion protein (CI), P3N-PIPO and the second 6 kDa protein (6K2) protein are essential for cell-to-cell movement of potyviruses (10). P3N-PIPO is localized in the plasmodesmata and directs CI to form conical structures that are crucial for assistance of potyviral intercellular movement through plasmodesmata, which was shown for turnip mosaic virus (TuMV) in *Nicotiana benthamiana* (11). Accumulation of CP in plasmodesmata during infection is also crucial since together with the potyviral Helper-Component Proteinase (HCPro) increases the size exclusion limit (SEL) of

74 plasmodesmata, which was determined by microinjection studies for bean common mosaic
75 necrosis potyvirus (BCMNV) in *N. benthamiana* (12). Systemic infection encompasses viral
76 movement through phloem and less often through xylem to reach and infect plant distant tissues
77 (13, 14). However, before reaching vasculature, plant viruses need to cross various cellular barriers
78 including bundle sheath, vascular parenchyma and companion cells, to reach sieve elements,
79 through which they are transported to distant tissues (13). The invasion of distant tissues requires
80 unloading from sieve elements into companion cells and cell-to-cell movement into bundle sheath
81 and mesophyll cells (13). Despite PVY being one of the most extensively studied potyviruses on
82 molecular scale, information about crucial factors governing cell-to-cell as well as systemic spread
83 are scarce (5, 10).

84 The cryo-EM structures of some potyviruses including PVY, watermelon mosaic virus (WMV) and
85 TuMV virions have been determined and offered a detailed insight into the conserved helical
86 arrangement of CPs assembled around viral ssRNA as well as the conserved three dimensional
87 structure of CP among them (15, 16, 17). CP is the only potyviral structural protein and more than
88 2000 copies of CP encapsidate the viral ssRNA molecule to form potyviral virions (5, 9). Individual
89 CP is built of three distinct regions. The N terminal region with residues up to Val44 in PVY, which
90 are exposed at the outer surface of the virus, are flexible and thus its 3D structure was not
91 determined. The rest of N terminal region, from Val44 to Gln76, is structured. It has an extended
92 structure with one short alpha helix in the middle (15). The central core has a globular shape. The
93 C terminal region is in the lumen of the virus and its extended structure is supported by the viral
94 ssRNA scaffold (15). Beyond its primary role in viral encapsidation, the CP is indispensable for
95 aphid transmission, potyviral RNA amplification and cell-to-cell movement (9, 12, 18). Functional
96 studies of the CP protein indicate crucial roles of its N and C terminal regions and the core region
97 in potyvirus infectivity. In the case of PVY, the absence of the flexible CP N terminal region hinders
98 the formation of filaments and cell-to-cell viral movement (15). For soybean mosaic virus (SMV),
99 the CP C terminal region is involved in CP intersubunit interactions, viral cell-to-cell and long
100 distance movement and virion assembly (19). In potato virus A (PVA), phosphorylation of Thr243

101 residue on CP C terminal region is crucial for PVA replication *in planta* (20). These results and
102 results of several other studies suggest that different CP regions are important for cell-to-cell
103 movement of potyviruses (21, 22, 23, 24, 25, 26). It is not known yet in what structural shape are
104 the viruses propagated through the plant, as assembled virions or viral ribonucleoprotein (RNP)
105 complexes associated with CP (13, 14).

106 The so far generated evidence-based knowledge differs from one potyvirus to another, and thus,
107 more research is needed to comprehensively elucidate these complex processes, particularly for
108 those economically relevant potyviruses such as PVY. By constructing different PVY N terminal
109 deletion mutants, we identified the regions of the CP that are important for efficient PVY cell-to-cell
110 movement and putative mechanisms supporting it. Moreover, by observing constructed deletion
111 mutants under TEM we explored the efficiency of deletion mutants to assemble into full virions.

112

Results

Deletion of 40 or more amino acid residues from the PVY CP N terminal region affects cell-to-cell movement, but does not prevent replication

Previously we showed that PVY with deleted 50 N terminal amino acid residues was still able to replicate but based on the low and spatially limited levels of RNA accumulation, we suggested that N terminal region is required for cell-to-cell movement (15). To confirm this hypothesis, we here constructed two GFP-tagged PVY (PVY N605-GFP) mutants lacking either 40 or 50 amino acid residues at the CP N terminal region (hereafter ΔN50-CP and ΔN40-CP). In all constructed mutants GFP was inserted between NIb and CP coding sequence, flanked by protease recognition sites, allowing GFP excision from the polyprotein after translation (27). We followed the spread of ΔN50-CP and ΔN40-CP with confocal microscopy upon bombardment of *Nicotiana clevelandii* leaves (Fig. 1B). Neither mutant was able to move cell-to-cell, remaining limited to bombarded cells (Fig. 1B). We detected viral RNA multiplication of both mutants in the bombarded leaves, albeit at significantly lower levels in comparison to the non-mutated clone (hereafter WT-CP) (Fig. S1, data S1 and S2). These findings corroborate our previous results showing that N terminal region CP truncations still allow viral replication (15) and further show that the absence of either 50 or 40 N-terminal residues abolish cell-to-cell viral movement.

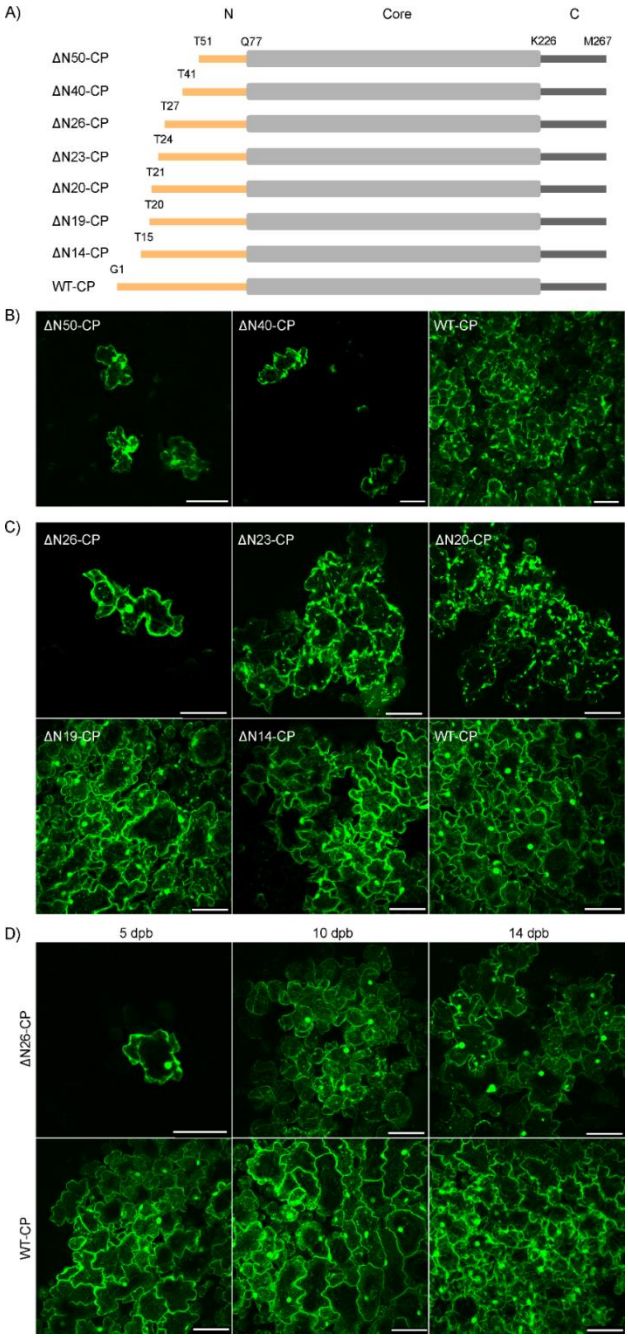

Figure 1. Amino acid deletions at PVY CP N terminal region influence viral cell-to-cell movement. **(A)** Schematic representation of constructed mutants with deletions on PVY CP N terminal region (N-terminal region, orange; core region, grey; C-terminal region, dark grey) with labeled amino acids. **(B)** Confocal microscopy images showing viral replication is limited to single cells when 50 (ΔN50-CP) or 40 (ΔN40-CP) amino acid residues were deleted at CP N terminal region, while non-mutated clone (WT-CP) shows cell-to-cell spread 10-12 days post bombardment (dpb). Scale bar: 100 μm. **(C)** 5 dpb viral replication is limited to

141 single cells in ΔN26-CP mutant, while cell-to-cell virus spread was observed for CP deletion mutants ΔN23-
142 CP, ΔN20-CP, ΔN19-CP, ΔN14-CP. Scale bar: 100 µm. **(D)** ΔN26-CP cell-to cell-spread was observed at later
143 time points (10 and 14 dpb). Scale bar: 100 µm.

144 **The deletions of 19-26 amino acid residues of the PVY CP N terminal region are influencing**
145 **dynamics of viral cell-to-cell spread**

146 To further assess which region of CP N terminal is crucial for cell-to-cell virus spread, we
147 constructed GFP-tagged mutants lacking 26, 23, 20, 19 and 14 amino acid residues at the CP N
148 terminal region (Fig. 1A) and followed their localization under confocal microscope at different time
149 points after virus inoculation (Fig. 1, C and D, data S2 and table S1). Mutants lacking 26 (ΔN26 -
150 CP) and 23 (ΔN23 -CP) residues on CP N terminal region had the first non deleted amino acid
151 replaced with glycine (G) during the mutagenesis.

152 At 5 dpb, ΔN14-CP and ΔN19-CP mutants did not show any differences in cell-to-cell spread
153 compared to WT-CP, while a lower spread level was noticed for ΔN20-CP and ΔN23-CP (Fig. 1C).
154 The most pronounced difference in comparison to other mutants and to WT-CP was observed in
155 the case of ΔN26-CP mutant, which remained confined to single cells at 5 dpb (Fig. 1, C and D).
156 However, at later time points (10 and 14 dpb), in approximately half of the infected plants, we also
157 observed cell-to-cell viral movement, although substantially delayed compared to WT-CP (Fig. 1D
158 and table S1). Also, the measured viral RNA load for ΔN26-CP mutant was significantly lower than
159 that of WT-CP at all 5 dpb, 10 and 14 dpb (fig. S2 and data S1).

160 Whole plant imaging was conducted to more precisely examine the dynamics of cell-to-cell virus
161 spread of WT-CP, ΔN23-CP, ΔN19-CP and ΔN14-CP through time on inoculated *N. clevelandii*
162 leaves (Fig. 2A). As expected, the results revealed statistically significant differences in the viral
163 multiplication area between N23-CP and WT-CP, and ΔN19-CP compared to WT-CP (Fig. 2, B and
164 C and data S3 and S4). A similar though less evident trend was observed in the case of ΔN14-CP
165 compared to WT-CP, which was not statistically significant (Fig.2 C and data S4).

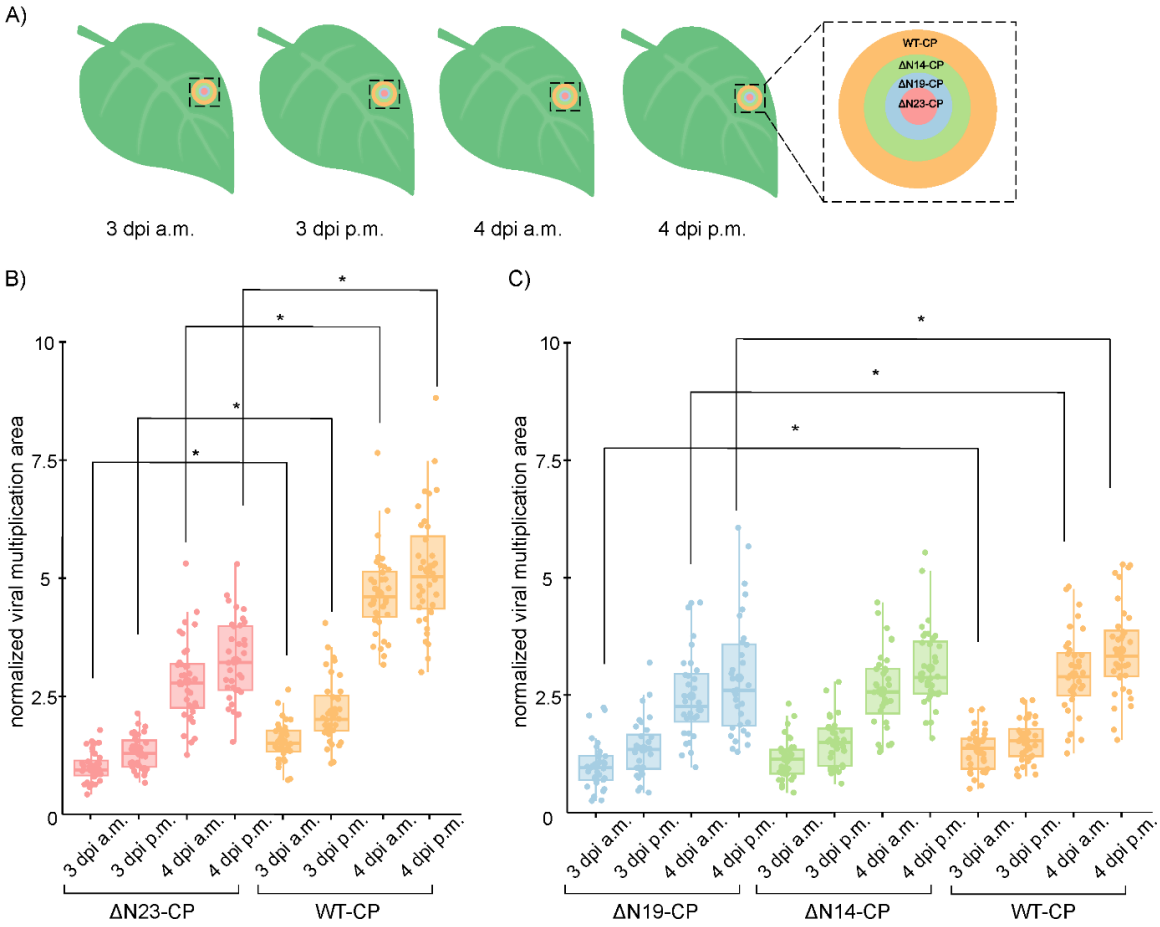

Figure 2. Precise analysis of the viral multiplication areas revealed a hampered cell-to-cell virus spread in ΔN19-CP and ΔN23-CP mutants. (A) The scheme of the viral multiplication area at different time points for all mutants compared with WT-CP. The area was followed by more precise analysis using whole plant imaging system for examining cell-to-cell virus spread of ΔN23-CP, ΔN19-CP, ΔN14-CP and WT-CP in four timepoints including 3 days post inoculation (dpi) in the morning (a.m), 3 dpi in the afternoon (p.m), 4 dpi a.m. and 4 dpi p.m. Note that the viral multiplication area was the largest after infection with WT-CP and decreased in the latter order ΔN14-CP, ΔN19-CP and ΔN23-CP. **(B and C)** Normalized viral multiplication area. After inoculating leaves with WT-CP or mutants, plants were imaged with whole plant imaging system. Images of three selected viral multiplication areas per leaf per plant were taken at four time points. Differences were statistically evaluated using Welch's t test. Results are presented as boxplots with dots representing normalized viral multiplication areas (data S3 and S4) for ΔN23-CP-CP, WT-CP **(B)** and ΔN19-CP, ΔN14-CP, WT-CP **(C)**. Statistically significant differences ($p < 0.05$) are denoted with an asterisk (*). Vertical lines present all points except outliers. Raw and normalized data, number of plants and statistics are specified in Data S3

180 and S4. The same trend was observed in a replicate experiment (fig. S3 and data S5). For comparison
181 between two independent experiments, data measured for mutant viruses were normalized to median of
182 values obtained for WT virus (data S6).

183 These results show that the dynamics of viral cell-to-cell spread is dependent on the length of the
184 CP N terminal region (Fig. 1 and data S2). More precisely, as the number of CP N terminal region
185 deleted amino acid residues increases, cell-to-cell movement speed is decreased (Fig. 2, B and C
186 and data S3, S4 and S6). We conclude that amino acids in the region 19-26 on CP N terminal
187 region are essential for an optimal PVY cell-to-cell movement.

188 **Systemic viral spread dynamics is affected by the cell-to-cell movement**

189 Since viral cell-to-cell spread is prerequisite for systemic viral spread, we further tested if the
190 observed delay in cell-to-cell viral spread of mutants (Figs. 1, C and 2, B and C) affects the systemic
191 viral spread. In contrast to the systemic spread of WT-CP, which is detectable already at 7 dpb, the
192 spread of ΔN23-CP, ΔN19-CP and ΔN14-CP mutants to systemic leaves occurs with a delay (Fig.
193 3A). If compared to WT-CP, ΔN14-CP was observed in systemic tissue with 1 day delay (8 dpb),
194 ΔN19-CP with 2 days delay (9 dpb) and ΔN23-CP with approximately 3 weeks delay (25 dpb) (Fig.
195 3A). The mutant ΔN26-CP did not reach systemic leaves even at the highest tested dpb.

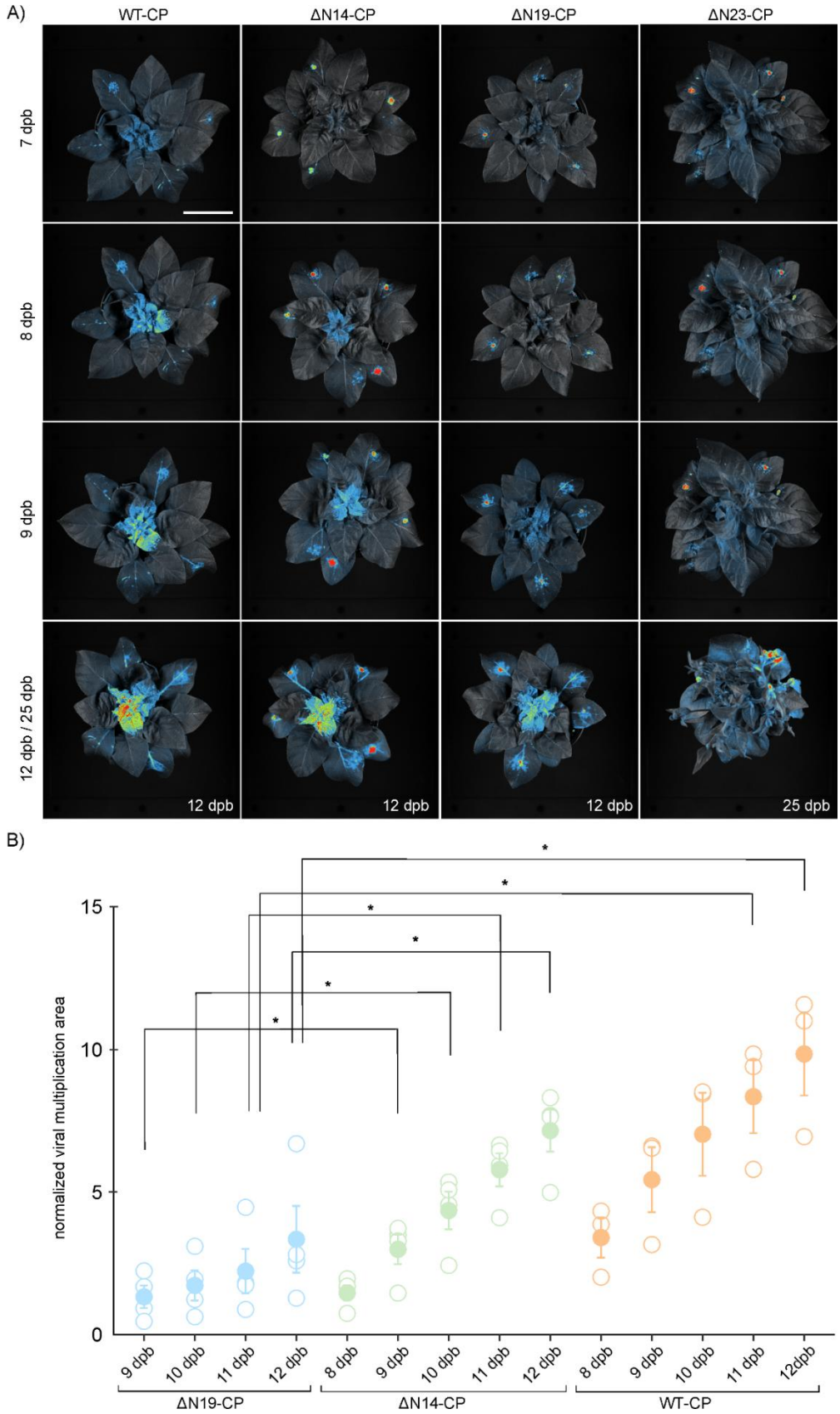
A)
WT-CP
ΔN14-CP
ΔN19-CP
ΔN23-CP
7 dpb
8 dpb
9 dpb
12 dpb / 25 dpb
12 dpb
12 dpb
12 dpb
25 dpb
B)
normalized viral multiplication area
15
10
5
0
9 dpb
10 dpb
11 dpb
12 dpb
8 dpb
9 dpb
10 dpb
11 dpb
12 dpb
8 dpb
9 dpb
10 dpb
11 dpb
12dpb
ΔN19-CP
ΔN14-CP
WT-CP

Figure 3. Systemic viral spread of mutants is delayed similarly as cell-to-cell movement. (A) Spatio-temporal PVY distribution in *N. clevelandii* systemic tissue. Viral multiplication area was followed 7-12 and 25 days post bombardment (dpb), by using whole plant imaging system. Scale bar: 5 cm. **(B)** Quantification of viral multiplication area in ROI in the *N. clevelandii* systemic tissue in total count per mutant in five selected timepoints including 8-12 dpb. Since ΔN19-CP did not spread systemically at 8 dpi, normalized viral multiplication area is not shown. Mean (represented with filled dot) and standard error are shown. Individual measurements are shown as empty dots, representing normalized viral multiplication area. Differences were statistically evaluated using Welch`s t test. Statistically significant differences ($p < 0.05$) are marked with asterisk. Raw and normalized data, number of plants and statistics are specified in data S7. Since ΔN26-CP is not capable of spreading systemically, it was not included in the analysis. Also ΔN23-CP had such a delayed spread that it was not possible to do a quantification of viral multiplication area at 8 to 12 dpb (Fig. 3A).

Quantitative analysis of viral multiplication signal in systemic tissue confirmed that WT-CP achieved the largest multiplication area, followed by ΔN14-CP and lastly ΔN19-CP in all observed time points (Fig. 3 and data S7). When comparing ΔN14-CP and WT-CP, we observed a trend of slower spread in case of ΔN14-CP, albeit not statistically significant (Fig. 3B and data S7). ΔN23-CP was not included in the comparison, due to the considerable delay in the systemic spread exhibited by this mutant (Fig. 3A), which made it difficult to measure the viral multiplication area. In conclusion, systemic viral spread is abolished for ΔN26-CP, and decreasingly hampered in case of ΔN23-CP, ΔN19-CP, while ΔN14-CP mutant is able to move similarly as WT-CP, albeit with a short delay.

Efficiency of assembly into full length viral particles is dependent on N terminal region of CP

In order to check the efficiency of virion assembly, we observed WT-CP and constructed deletion mutants ΔN14-CP, ΔN19-CP, ΔN23-CP, ΔN26-CP and ΔN50-CP under TEM and analyzed the viral particle lengths with ImageJ software (NIH). Note that we were not able to measure viral particles lengths of ΔN40-CP deletion mutant due to particles aggregation (Fig. 4A).

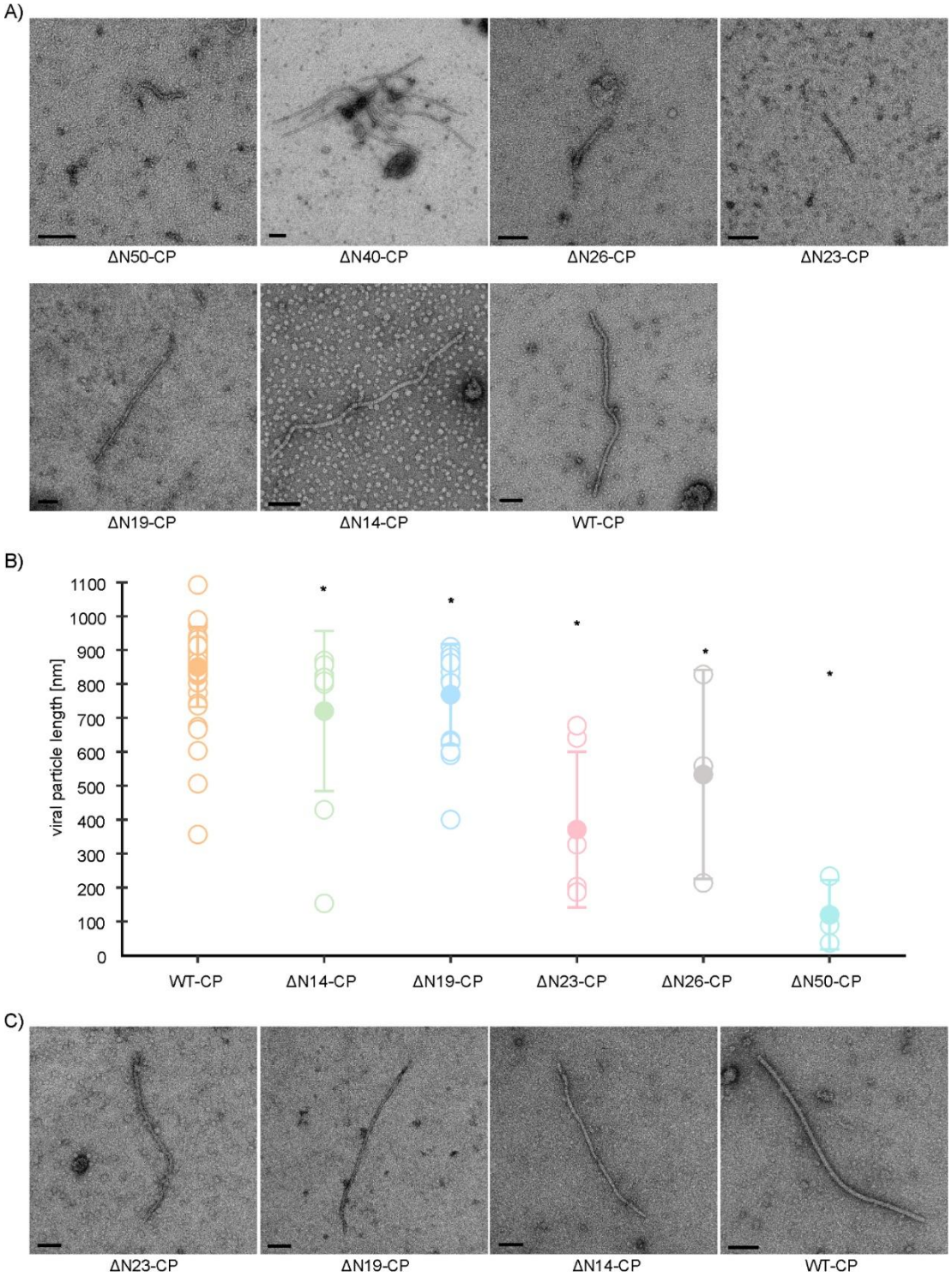

223

224 **Figure 4. Assembly of viral particles. (A)** Abolished formation of full length viral particles in deletion

225 mutants in bombarded leaves. Scale is 100 nm. **(B)** Distribution of viral particles lengths in bombarded

226 leaves. Observed statistically significant differences between deletion mutants and WT-CP using Kruskal-
227 Wallis test, are marked with an asterisks (*). Mean (represented with filled dot) and standard deviation are
228 shown. Individual measurements are shown as empty dots, representing normalized viral multiplication area.
229 See data S8 for more statistical testing. We were not able to measure viral particles lengths in case of
230 ΔN40-CP due to particle aggregation. **(C)** Formation of full length viral particles in systemic leaves. Note
231 that we were not able to observe ΔN50-CP, ΔN40-CP nor ΔN26-CP viral particles in systemic leaves, since
232 they are not capable of spreading systemically. Scale is 100 nm. Representative micrographs of viral
233 particles for deletion mutants were obtained with negative staining TEM in bombarded and systemic leaves.
234 See Materials and methods section and data S2 for more details.

235 Analyzed deletion mutants ΔN14-CP, ΔN19-CP, ΔN23-CP, ΔN26-CP and ΔN50-CP formed
236 shorter viral particles if compared to WT-CP, since statistically significant results were observed
237 between WT-CP and all tested deletion mutants (Fig. 4B and data S8). The shortest viral particle
238 lengths were measured in case of ΔN50-CP deletion mutant and were statistically significantly
239 shorter in comparison to ΔN19-CP, ΔN14-CP (data S8). On the other hand, by the mutants with
240 shorter deletions (ΔN14-CP, ΔN19-CP, ΔN23-CP, ΔN26-CP) the trend of longer viral particles in
241 comparison to ΔN50-CP, albeit shorter than WT-CP was observed (Fig. 4, A and B and data S8).
242 To sum up, CP N terminal region deletions are influencing the efficiency of viral particles
243 assembly (Fig. 4, A and B). As expected, full length viral particles were detected in systemic
244 leaves in case of ΔN19-CP and ΔN14-CP at 22 dpb, while we could not find them in case of
245 ΔN26-CP, which is not capable of spreading systemically (Fig. 4C).

246 **Change of flexibility in N-terminal region affects cell-to-cell viral movement**

247 To pinpoint amino acids important for cell-to-cell virus movement, we generated point mutations in
248 the CP N terminal region, for charged residues Asp14, Glu18, for potential phosphorylation site at
249 Ser21 and for 3D structure breakers Gly20 and Pro24. Selected residues were changed to Ala
250 (D14A, E18A, P24A), except for Ser21 where the sequence coding for Ala and Thr substitution was
251 unstable in *E. coli*, thus we mutate is to Gly (S21G) and for Gly20, where we intentionally introduced
252 Pro (G20P) to affect the fold of N terminal region (Fig. 5A).

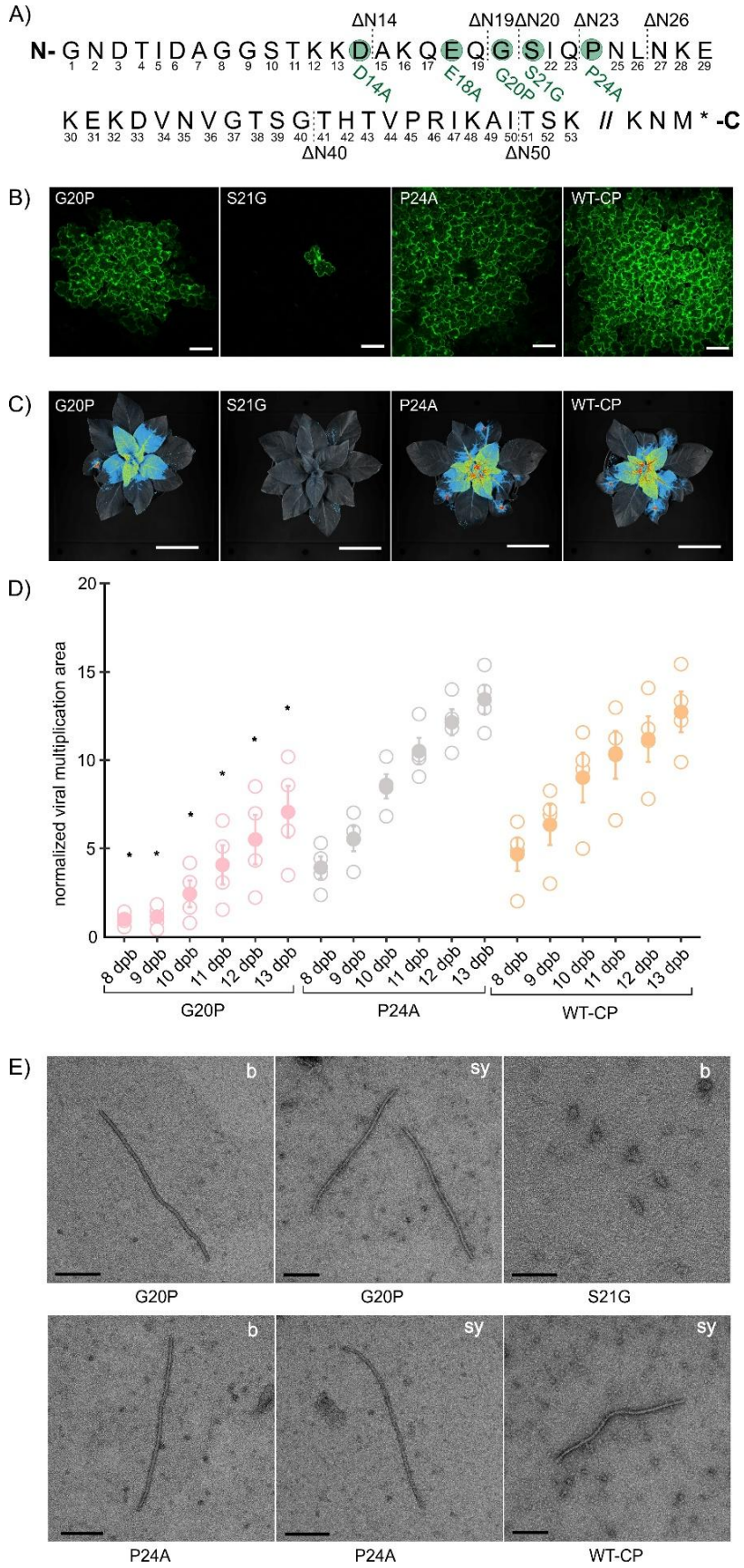
A)
ΔN14
ΔN19
ΔN20
ΔN23
ΔN26
N- G N D T I D A G G S T K K D A K Q E Q G S I Q P N L N K E
D14A
E18A
G20P
S21G
P24A
K E K D V N V G T S G T H T V P R I K A I T S K // K N M * -C
ΔN40
ΔN50
B)
G20P
S21G
P24A
WT-CP
C)
G20P
S21G
P24A
WT-CP
D)
normalized viral multiplication area
8 dpb
9 dpb
10 dpb
11 dpb
12 dpb
13 dpb
G20P
P24A
WT-CP
E)
b
sy
G20P
G20P
S21G
P24A
P24A
WT-CP

253

254 **Figure 5. Substitution of serine to glycine on position 21 of CP N terminal region abolished cell-to-**
255 **cell viral movement and virion assembly. (A)** Amino acid sequence of GFP tagged infectious clone PVY-
256 N605(123) CP protein with labeled constructed deletion and point mutants. The scheme presents mutants
257 with deletions of 14 (ΔN14-CP), 19 (ΔN19-CP), 20 (ΔN20-CP), 23 (ΔN23-CP), 26 (ΔN26-CP), 40 (ΔN40-CP)
258 or 50 (ΔN50-CP) amino acids on CP N terminal region and mutants with point mutations including
259 substitutions of negatively charged aspartic acid to alanine on position 14 (D14A), negatively charged
260 glutamic acid to alanine on position 18 (E18A), glycine to proline on position 20 (G20P), serine to glycine on
261 position 21 (S21G) and proline to alanine on position 24 (P24A). **(B)** Confocal microscopy images showing
262 viral cell-to-cell spread of mutants G20P, S21G, P24A and WT-CP 5 dpb. Scale is 100 µm. **(C)** Spatio-
263 temporal PVY distribution for constructed point mutants G20P, S21G, P24A and WT-CP in *N. clevelandii*
264 systemic tissue as observed by whole plant imaging system 12 dpb. Scale is 5 cm. **(D)** Quantification of viral
265 multiplication area in the upper systemic leaves of bombarded *N. clevelandii* in 6 selected timepoints (8-13
266 dpb). Mean (represented with filled dot) and standard error are shown. Individual measurements are shown
267 as empty dots, representing normalized viral multiplication area. Differences between analyzed point
268 mutants were evaluated with Welch`s t test. Statistically significant differences ($p<0.05$) between G20P
269 mutant and WT-CP are represented with asterisks (*), while there were no statistically observed differences
270 between P24A and WT-CP (see data S9 for all results of statistical testing). Vertical lines present all points
271 except outliers. The results were confirmed in additional experiments (Fig. S4 and data S10). **(E)**
272 Representative TEM micrographs of point mutants in bombarded (b) and systemic (sy) leaves 13 dpb.
273 Results were obtained with negative staining. Scale bars are 200 nm, except in case of S21G (50 nm).

274 Viral cell-to-cell spread of mutants D14A, E18A and P24A was comparable to WT-CP (Fig. 5B and
275 S5). On the other hand, G20P mutant showed delayed cell-to-cell spread, while S21G mutant
276 remained limited to just single cells at all observed timepoints (Figs. 5B and S5).

277 Next, we performed whole plant imaging to study systemic viral spread of mutants (Figs. 5C and
278 S7). In accordance with the results of cell-to-cell movement, there were no statistically significant
279 differences in viral multiplication area in systemic tissue when comparing D14A, E18A or P24A with
280 WT-CP (Figs. 5D, S6, S4 and data S9, S10, S11, S12) at all observed timepoints. On the other
281 hand, the viral multiplication area of G20P in systemic tissue was statistically significantly lower
282 compared to WT-CP at all observed time points (Fig. 5D and data S9). As expected, S21G did not

spread systemically (Fig. 5C). Furthermore, electron microscopy showed the ability of E18A, G20P and P24A to form viral particles as WT-CP in both, bombarded and systemic leaves, while we were not able to find any viral particles in case of S21G, however, we observed oligomeric rings which could be connected into very short fragments (Fig. 5E). We conclude that fold altering mutations in the 19-26 region of interest, hinder the formation of filaments (S21G) and prevent (S21G) or delay (G20P) the movement of PVY.

Discussion

The biological function of C and N terminal regions of PVY CP has already been initiated in our previous study, where we hypothesized that N terminal amino acid residues are necessary for an efficient cell-to-cell movement (15). Here we provide additional insights into the mechanism of PVY spread by identifying the regions of PVY CP N terminal region that are important for efficient viral cell-to-cell movement and systemic infection.

Despite the conserved flexible structure of potyviruses N terminal region of CP, there are notable differences observed regarding its involvement in potyviral cell-to-cell and systemic movement. In the case of zucchini yellow mosaic virus (ZYMV), deletion of the entire CP N terminal region did not affect systemic infection (22). Similarly, a deletion of 6-50 amino acids in the CP N terminal domain did not compromise TuMV cell to cell and systemic movement (18). On the other hand, in tobacco etch potyvirus (TEV), CP N terminal region deletions of 5-29 amino acid residues delayed cell-to-cell movement and prevented systemic spread (21). We observed inability to move cell-to-cell for PVY when 40 or more amino acid residues were deleted from CP N terminal region (Fig. 1). However, shorter deletions in the range of 19 to 23 did not prevent systemic spread but resulted in delayed systemic and cell-to-cell PVY movement (Figs. 2, B and C, 3B and data S4, S3 and S7). The reason behind these observed differences among different potyviral species may be in phylogeny, since ZYMV belongs to bean common mosaic virus (BCMV) supergroup of potyviruses while TEV, PVY and interestingly TuMV as well, to the PVY supergroup (28, 29).

309 The analysis of viral multiplication area revealed important insights into the cell-to-cell movement
310 dynamics of deletion mutants, as increasing number of deleted amino acid residues at CP N
311 terminal region resulted in slower cell-to-cell viral spread (Fig. 2, B and C). Furthermore, slower
312 cell-to-cell virus spread also impacted infection of systemic tissue (Fig. 3A). The connection
313 between cell-to-cell movement and systemic spread was expected, as the virus reaches the veins,
314 enters the veins and is transported in systemic tissue with a delay due to decelerated cell-to-cell
315 movement (30).

316 Results of several studies suggested the role of charged amino acids in the CP core and C terminal
317 region of different potyviruses in cell-to-cell and systemic virus spread (18, 19, 25). In contrast,
318 results of our study show that the role of charged amino acids in the CP N terminal region of PVY
319 is not significant, as cell-to-cell spread of D14A and E18A mutants was comparable to WT-CP (Fig.
320 5B).

321 On the other hand, we observed that replication of S21G mutant was limited to single cells (Fig.
322 5B), which might be due to loss of potential phosphorylation site or disruption of N-terminus
323 structure, due to introduction of glycine. Note that to confirm the hypothesis about the important
324 potential role of phosphorylation of Ser21, we aimed to replace Ser21 also with alanine and
325 threonine, but the design of such point mutants was not achievable, due to their instability in *E. coli*.
326 It has been previously suggested that PVY cDNA is unstable in *E. coli*. Stability of full length PVY
327 plasmids was achieved by inserting introns into putatively toxic genes but still for some mutants
328 recombinations can occur (31).

329 Furthermore, we also showed the important role of the glycine on position 20 of CP N terminal
330 region in PVY cell-to-cell as well as systemic spread, since G20P mutant spreads slower than WT-
331 CP (Fig. 5 B, C and D). We hypothesize that exchanging Gly with Pro in G20P mutant increased
332 rigidity to the N terminal region. This alteration was apparently not enough as to prevent virus
333 assembly (Fig. 5E). However, the mutation may have impacted the interaction of the CP with other
334 host and viral proteins in the cell resulting in the observed delay.

335 Our study suggests that CP N terminal region is also important for efficiency of assembly into full
336 length viral particles, since viral lengths of observed deletion mutants ΔN14-CP, ΔN19-CP, ΔN23-
337 CP, ΔN26-CP and ΔN50-CP were statistically significantly shorter if compared to WT-CP (Fig. 4B).
338 Furthermore, electron microscopy (EM) observations indicate that deletion of 50 or 40 amino acids
339 on PVY CP N terminal region are not only preventing cell-to-cell movement, but impact virion
340 formation as well (Fig. 4A), since with ΔN50-CP mutant we saw only shorter fragments, while in
341 case of ΔN40-CP virions were formed to similar lengths as WT-CP virions, with apparently higher
342 tendency to aggregate (Fig. 4A). This is partially in accordance with (18), who observed aberrant
343 TuMV virions in case 6-50 amino acids deletion of TuMV CP N terminal region. Interestingly, in
344 contrast with our results, this deletion did not significantly compromise TuMV cell-to-cell and
345 systemic movement (18).

346 Intact PVY CP N terminal region is important for correct virion formation and for an optimal PVY
347 movement, unlike in some other potyviruses. Since we observed properly formed virions also in
348 case there was a delay in movement (G20P) (Fig. 5E), we speculate that interaction of N terminal
349 region, which is disordered with some other proteins is required for efficient PVY spread. We also
350 show the importance of CP N terminal region for efficiency of assembly into full length viral particles.
351 The results identifying crucial domains and amino acids of CP N terminal region in viral cell-to-cell
352 movement provided in our study are important basis to elucidate these complex processes,
353 particularly in most economically important viruses such as PVY.

354

Materials and Methods

Plant material

N. clevelandii plants were used to follow virus spread. Plants were grown from seeds and kept in growth chambers under controlled conditions as described previously (32).

Construction of PVY-N605(123)-GFP CP N-terminal deletion and point mutants

As a template to construct mutants with deletions on the CP N terminal region, we used a GFP-tagged infectious clone PVY-N605(123) constructed by (27). The GFP coding sequence was inserted between NIb and CP coding sequences, flanked by protease target sequences, so that GFP would not bother viral movement, since it is excised from the polyprotein as other viral proteins (27). Megaprimers were designed in accordance with instructions prepared by (33). Detailed information about mutagenic PCR reactions conditions and mixtures can be found in Text S1. After adding 4 µL of *DpnI* enzyme, the mutagenesis mixtures were transformed into *E. coli* XL 10 Ultracompetent Cells in accordance with manufacturer`s instructions (Agilent Technologies). Transformation mixtures were plated on LB agar with ampicillin selection and incubated overnight at 37ºC. Transformants were screened with colony PCR using PVY GFP_F and PVY uni_R primers (data S13) and KAPA2G Robust HotStart Kit (Agilent Technologies). Prior bombardment, polyprotein and its promoter in PVY-N605(123) lacking 50 and 14 amino acids on CP N-terminus were Sanger sequenced (data S13) Additionally, restriction analysis was performed to confirm the correctness of the PVY coding region.

Biolistic bombardment

Constructed PVY mutants and wild type plasmids were amplified in *E. coli*. Plasmids were then isolated and coated onto gold microcarriers that were used for *Nicotiana clevelandii* bombardment using a Helios® gene gun (Bio-Rad), as described by (33).

381 **Plant material sampling and RNA isolation**

382 Plant leaf samples were collected from bombarded *N. clevelandii* plants by excising 0,3 g plant
383 tissue near the bombardment site. Sampled plant material from bombarded *N. clevelandii* leaves
384 was homogenized in 700 µl of RNeasy kit RLT lysis buffer with FastPrep (MP Biomedicals) 1 min
385 6,5 m/s. Total RNA was isolated using RNeasy Plant Mini Kit (Qiagen). Residual DNA was digested
386 with deoxyribonuclease I (DNase I, Qiagen) in solution, using 1.36U DNase/µg RNA. Quality control
387 of isolated RNA was performed as described in (32).

388 **RT-qPCR**

389 Relative PVY RNA concentration was determined by single-step quantitative RT-PCR (RT-qPCR;
390 AgPath-ID One-Step RT-PCR, Thermo FisherScientific) for the ΔN50-CP mutant, while two step
391 RT-qPCR was performed for other mutants. RNA was reverse transcribed with High-Capacity cDNA
392 Reverse Transcription Kit (Thermo Fisher Scientific) and analyzed by qPCR using FastStart
393 Universal Probe Master (Roche).

394 A qPCR assay targeting the PVY CP encoding region was used as a target gene, while the gene
395 encoding for cytochrome oxidase (COX) was used as reference gene. To avoid false positive
396 results plants bombarded with plasmid encoding for blue fluorescent protein, were sampled and
397 analyzed with our qPCR assay targeting PVY CP encoding region. RT-qPCR amplification program
398 and reaction composition mixtures were the same as in (27). Primers and Probes details are listed
399 in data S13.

400 After conducting RT-qPCR reactions, the QuantGenius software (34) was used for relative
401 quantification of PVY RNA using the standard curve approach. Data containing information about
402 the relative RNA quantity, was averaged for each group and then normalized to the lowest group
403 average number (data S1).

404

405

406 **RT-PCR**

407 One-step reverse transcription PCR (QIAGEN OneStep RT-PCR Kit) was performed to confirm that
408 the introduced mutations were maintained in the viral progeny of all constructed mutants. DNAse-
409 treated RNA, isolated from leaves according to the above protocol, was used as a template.
410 Mutated region was amplified with PVY-GFP_F and uniPVY_R primers (data S13). The purified
411 PCR products were sequenced (Sanger sequencing). For samples with a small amount of mutated
412 virus (ΔN50-CP, ΔN40-CP, S21G), an additional PCR (repliQa HiFi ToughMix; Quantabio) on
413 purified products was performed to amplify the mutated region in sufficient quantity.

414 **Confocal microscopy**

415 Cell-to-cell viral spread on upper side of bombarded *N. clevelandii* leaf discs, sampled with cork
416 borer, was observed under Leica TCS LSI confocal macroscope with Plan APO x5 and x20
417 objectives (Leica Microsystems, Wetzlar, Germany) at different time points (5-14 dpb), and Stellaris
418 5 confocal microscope with HC PL FLUOTAR x10 objective (Leica Microsystems, Wetzlar,
419 Germany) for studying point mutations at 5 dpb. The GFP emission was recorded after excitation
420 with 488 nm laser in the window between 505 and 530 nm and used as a direct measure of the
421 presence of metabolically active viruses in the observed tissue. Sampled discs were scanned
422 unidirectionally with scan speed of 400 Hz and frame average 1 or 2. For following the spread of
423 ΔN50-CP at 12 dpb, ΔN40-CP and WT-CP at 10 dpb, 5x objective was used (Fig. 1B), while for
424 following the spread of ΔN26-CP, ΔN23-CP, ΔN20-CP, ΔN19-CP, ΔN14-CP mutants and WT-CP at
425 5 dpb, 20x objective was used (Fig. 1, C and D,). Images were processed using LEICA LAS X
426 software (Leica microsystems) to obtain maximum projections from z-stacks.

427 **EM sample preparation**

428 The presence of viral particles, compactness of structure and particle length were assessed with
429 transmission electron microscopy (TEM) using negative staining method. Tissue extracts were
430 prepared from leaf discs, in which viral presence was previously confirmed with confocal
431 microscope, and then macerated in phosphate buffer (0.1 M, pH 6.8). 20 µL of extracts were applied

432 to a grid for 5 minutes, blotted, washed, and stained with 1% (w/v) water solution of uranyl acetate.
433 Grids were observed by TEM TALOS L120 (Thermo Fisher Scientific) operating at 100 kV or 120
434 kV. Micrographs were recorded using Ceta 16 M camera and software Velox (Thermo Fisher
435 Scientific).Viral particle lengths of WT-CP and ΔN14-CP, ΔN19-CP, ΔN23-CP, ΔN26-CP and ΔN50-
436 CP deletion mutants were measured with ImageJ software (NIH).

437 **Virus inoculation**

438 To more precisely examine cell-to-cell viral movement by whole plant imaging, we inoculated 3-4
439 weeks old *N. clevelandii* plants with inoculum prepared from systemic leaves of ΔN14-CP, ΔN19-
440 CP, ΔN23-CP and WT-CP-inoculated plants in which GFP signal was confirmed using whole plant
441 imaging system. Systemic leaves were ground in phosphate buffer (supplemented with PVP 10000)
442 in a plant material : buffer ratio of 1:4. Three bottom leaves of *N. clevelandii* plants were dusted
443 with carborundum powder and rubbed with the inoculum (1-3 drops of inoculum per leaf) which was
444 removed after 10 min by rinsing with tap water.

445 **Whole plant imaging**

446 Cell-to-cell and systemic viral spread throughout the plant was monitored using the Whole plant
447 imaging system Newton 7.0 BIO (Vilber) in bombarded and inoculated *N. clevelandii* plants. GFP
448 emission of GFP-tagged PVY clone was followed in 480 nm excitation channel and emission filter
449 F-550. Images were taken by EvolutionCapt edge software. For viral multiplication area analysis in
450 inoculated leaves, all three ΔN14-CP-, ΔN19-CP-, ΔN23-CP- and WT-CP-inoculated leaves of *N.*
451 *clevelandii* were imaged using exposure time 1 min 46 sec 700 msec, 10x10 field of view (FOV)
452 and 1331-1337 focus in 4 time points: 3 dpi a.m. and p.m. and 4 dpi a.m. and p.m. For studying
453 systemic viral spread, ΔN14-CP-, ΔN19-CP-, ΔN23-CP and WT-CP-bombarded *N. clevelandii*
454 plants were imaged, using 50 s exposure time, 20x20 FOV and focus in the range between 1871
455 and 1905 in different time points (4-32 dpb). For studying systemic viral spread of point mutations,
456 plants were imaged at different time points (6-13 dpb) with exposure time 5 s and 50 s and other
457 settings as for studying systemic viral spread of deletion mutants (see above). In case of

458 experiment with D14A and WT-CP at 13 dpb, exposure time was only 5 s to avoid saturation due
459 to a high signal.

460 **Image analysis and signal quantification following whole plant imaging**

461 Viral multiplication area analysis on inoculated leaves and on upper systemic leaves were
462 performed using Kuant software (Vilber, France). In case of viral multiplication area, surfaces of
463 three viral multiplication areas per leaf were measured, while in case of viral multiplication area in
464 systemic leaves, total count of the virus affected area was measured. Total count is determined as
465 a sum of gray values within region of interest (systemic leaves, ROI) and is proportional to the
466 intensity and spread of the signal. All measured data from Kuant software were exported to Excel,
467 where total count in ROIs were averaged for each timepoint and subsequently normalized on the
468 lowest group average number. Normalized viral multiplication areas were statistically evaluated
469 using Welch`s t-test and were used for graphic representation.

Acknowledgments

We thank Živa Lengar for technical support and laboratory assistance, Dr. Maja Zagorščak and Dr. Angelika Vižintin for help with statistical analysis.

References

1. Scholthof KBG, Adkins S, Czosnek H, Palukaitis P, Jacquot E, Hohn T, et al. Top 10 plant viruses in molecular plant pathology. Molecular Plant Pathology. 2011; 12: 938-954.

2. Quenouille J, Vassilakos N, Moury B. Potato virus Y: A major crop pathogen that has provided major insights into the evolution of viral pathogenicity. Molecular Plant Pathology. 2013; 14(5):439-452.

3. Ivanov KI, Eskelin K, Lõhmus A, Mäkinen K. Molecular and cellular mechanisms underlying potyvirus infection. Journal of General Virology. Society for General Microbiology. 2014; 95: 1415-1429.

4. Y-W Chung B, Allen Miller W, Atkins JF, Firth AE. An overlapping essential gene in the Potyviridae. Proc. Natl. Acad. Sci. USA. 2008; 105: 5897-5902.

5. Yang X, Li Y, Wang A. Research Advances in Potyviruses: From the Laboratory Bench to the Field. Annu. Rev. Phytopathol. 2021; 59: 1-29.

6. Benitez-Alfonso Y, Faulkner C, Ritzenthaler C, Maule AJ. Plasmodesmata: Gateways to Local and Systemic Virus Infection. MPMI. 2010; 23(11):1403-1412.

7. Folimonova SY, Tilsner J. Hitchhikers, highway tolls and roadworks: the interactions of plant viruses with the phloem. Current Opinion in Plant Biology. 2018; 43: 82-88.

8. Reagan BC, Burch-Smith TM. Viruses reveal the secrets of plasmodesmal cell biology. Molecular Plant-Microbe Interactions. 2020; 33: 26-39.

9. Revers F, García JA. Molecular biology of potyviruses. Advances in Virus Research. 2015; 92: 101-199.

10. Xue M, Arvy N, German-Retana S. The mystery remains: How do potyviruses move within and between cells? Molecular Plant Pathology. 2023; 24: 1560-1574.

11. Wei T, Zhang C, Hong J, Xiong R, Kasschau KD, Zhou X, et al. Formation of complexes at plasmodesmata for potyvirus intercellular movement is mediated by the viral protein P3N-PIPO. PLoS Pathogens. 2010; 6: e1000962.

12. Rojas MR, Zerbini FM, Allison RF, Gilbertson RL, Lucas WJ. Capsid Protein and Helper Component-Proteinase Function as Potyvirus Cell-to-Cell Movement Proteins. Vol. 237, Virology. 1997; 237: 283-295.

13. Navarro JA, Sanchez-Navarro JA, Pallas V. Key checkpoints in the movement of plant viruses through the host. In: Advances in Virus Research. 2019; 104: 1-64.

14. Mäkinen K, Hafrén A. Intracellular coordination of potyviral RNA functions in infection. Vol. 5, Frontiers in Plant Science. Frontiers. 2014; 5: 110.

15. Kežar A, Kavčič L, Polák M, Nováček J, Gutiérrez-Aguirre I, Žnidarič MT, et al. Structural basis for the multitasking nature of the potato virus Y coat protein. Sci. Adv. 2019; 5: eaaw3808.

16. Zamora M, Méndez-López E, Agirrezabala X, Cuesta R, Lavín JL, Amelia Sánchez-Pina M, et al. Potyvirus virion structure shows conserved protein fold and RNA binding site in ssRNA viruses. Sci. Adv. 2017; 3: eaao2182.

17. Cuesta R, Yuste-Calvo C, Gil-Cartón D, Sánchez F, Ponz F, Valle M. Structure of Turnip mosaic virus and its viral-like particles. Sci Rep. 2019; 9: 15396.

18. Dai Z, He R, Bernards MA, Wang A. The cis-expression of the coat protein of turnip mosaic virus is essential for viral intercellular movement in plants. Mol Plant Pathol. 2020; 21(9):1194-1211.

19. Seo JK, Vo Phan MS, Kang SH, Choi HS, Kim KH. The charged residues in the surface-exposed C-terminus of the Soybean mosaic virus coat protein are critical for cell-to-cell movement. Virology. 2013; 446: 95-101.

20. Lõhmus A, Hafrén A, Mäkinen K. Coat Protein Regulation by CK2, CPIP, HSP70, and CHIP Is Required for Potato Virus A Replication and Coat Protein Accumulation. J Virol. 2017; 91: e01316-16.

21. Dolja VV, Haldeman R, Robertson NL, Dougherty WG, Carrington JC. Distinct functions of capsid protein in assembly and movement of tobacco etch potyvirus in plants. EMBO Journal. 1994; 13(6):1482-1491.

22. Arazi T, Shiboleth YM, Gal-On A. A Nonviral Peptide Can Replace the Entire N Terminus of Zucchini Yellow Mosaic Potyvirus Coat Protein and Permits Viral Systemic Infection. J Virol. 2001; 75(14): 6329-6336.

23. Kimalov B, Gal-On A, Stav R, Belausov E, Arazi T. Maintenance of coat protein N-terminal net charge and not primary sequence is essential for Zucchini yellow mosaic virus systemic infectivity. Journal of General Virology. 2004; 85(11): 3421-3430.

24. Tatineni S, Kovacs F, French R. Wheat streak mosaic virus Infects Systemically despite Extensive Coat Protein Deletions: Identification of Virion Assembly and Cell-to-Cell Movement Determinants. J Virol. 2014; 88(2):1366-1380.

25. Tatineni S, French R. The C-terminus of Wheat streak mosaic virus coat protein is involved in differential infection of wheat and maize through host-specific long-distance transport. Molecular Plant-Microbe Interactions. 2014; 27(2): 150-152.

26. Tatineni S, Elowsky C, Graybosch RA. Wheat streak mosaic virus coat protein deletion mutants elicit more severe symptoms than wild-type virus in multiple cereal hosts. Molecular Plant-Microbe Interactions. 2017; 30(12): 974-983.

27. Lukan T, Županič A, Mahkovec Povalej T, Brunkard JO, Kmetič M, Juteršek M, et al. Chloroplast redox state changes mark cell-to-cell signaling in the hypersensitive response. New Phytologist. 2023; 237(2): 548-562.

28. Gibbs A, Ohshima K. Potyviruses and the digital revolution. Annu Rev Phytopathol. 2010; 48: 205-223.

29. Gibbs AJ, Hajizadeh M, Ohshima K, Jones RAC. The potyviruses: An evolutionary synthesis is emerging. Viruses. 2020; 22: 132.

30. Wang A. Dissecting the Molecular Network of Virus-Plant Interactions: The Complex Roles of Host Factors. Annual Review of Phytopathology. 2015; 53: 45-66.

31. Bukovinszki A, Götz R, Johansen E, Maiss E, Balázs E. The role of the coat protein region in symptom formation on Physalis floridana varies between PVY strains. Virus Res. 2007; 127: 122-125.

32. Baebler Š, Krečič-Stres H, Rotter A, Kogovšek P, Cankar K, Kok EJ, et al. PVY(NTN) elicits a diverse gene expression response in different potato genotypes in the first 12 h after inoculation. Mol Plant Pathol. 2009; 10(2): 263-275.

33. Stare K, Coll A, Gutiérrez-Aguirre I, Žnidarič MT, Ravnikar M, Kežar A, et al. Generation and in Planta Functional Analysis of Potato Virus Y mutants. Bio Protoc. 2020; 10: e3692.

34. Baebler Š, Svalina M, Petek M, Stare K, Rotter A, Pompe-Novak M, et al. QuantGenius: Implementation of a decision support system for qPCR-based gene quantification. BMC Bioinformatics. 2017; 18(1): 276.

35. Kogovšek P, Gow L, Pompe-Novak M, Gruden K, Foster GD, Boonham N, Ravnikar M, Single-step RT real-time PCR for sensitive detection and discrimination of Potato virus Y isolates. J Virol. 2008; 149: 1-11.

36. Weller SA, Elphinstone JG, Smith NC, Boonham N, Stead DE, Detection of Ralstonia solanacearum strains with a quantitative, multiplex, real-time, fluorogenic PCR (TaqMan) assay. Appl. Environ. Microbiol. 2000; 66: 2853-2858.

Supporting information captions

Supplementary Text S1. Construction of PVY-N605(123)- GFP CP N-terminal mutants
Fig. S1. ΔN50-CP ΔN40-CP viral replication.
Fig. S2. Viral replication ΔN26-CP.
Fig. S3. N19-CP_ΔN14-CP_WT-CP cell-to-cell spread dynamics.
Fig. S4. Independent experiment for point mutants G20P, P24A and WT-CP to check viral abundance.
Fig. S5. Cell-to-cell viral spread of D14A, E18A, G20P, S21G and P24A point mutants.
Fig. S6. Virus abundance D14A, E18A, WT-CP.
Fig. S7. Point mutants systemic spread.
Table S1. ΔN26-CP viral limitation on single cells or cell-to-cell spread.
Data S1 (Microsoft Excel format). Normalized qPCR data for constructed PVY mutants.
Data S2 (Microsoft Excel format). General sample information including sample name, plant and leaf number, date of putting plants into the soil, date of bombardment.
Data S3 (Microsoft Excel format). Viral cell-to-cell spread evaluation after *N. clevelandii* inoculation with constructed mutant ΔN23/G-CP and WT-CP.
Data S4 (Microsoft Excel format). Viral cell-to-cell spread evaluation after *N. clevelandii* inoculation with constructed mutants ΔN19-CP, ΔN14-CP and WT-CP.
Data S5 (Microsoft Excel format). Viral cell-to-cell spread evaluation after *N. clevelandii* inoculation with constructed mutants ΔN19-CP, ΔN14-CP and WT-CP in replicate experiment.
Data S6 (Microsoft Excel format). Foci analysis comparisons between experiments.
Data S7 (Microsoft Excel format). Systemic spread dynamic analysis.
Data S8 (Microsoft Excel format). Viral particles lengths.
Data S9 (Microsoft Excel format). Systemic viral spread of G20P and P24A point mutants.
Data S10 (Microsoft Excel format). Systemic viral spread of G20P and P24A point mutants in replicate experiment.
Data S11 (Microsoft Excel format). Systemic viral spread of D14A point mutant.
Data S12 (Microsoft Excel format). Systemic viral spread of E18A point mutant.
Data S13 (Microsoft Excel format). Primers and megaprimers sequences.